JOURNAL OF MATERIALS SCIENCE 31 (1996) 150–156

Silicon nitride ceramics with celsian as an additive

C. J. HWANG*§, R. A. NEWMAN‡
Ceramics and Advanced Materials Laboratory, and ‡Analytical Sciences Laboratory, The Dow Chemical Company, Midland, MI 48667, USA

Four different Si_3N_4 ceramics using 10 wt% celsian ($BaAl_2Si_2O_8$) as an additive, have been prepared by hot pressing. Different celsian sources and hot-pressing conditions were used and their effects on densification, *in situ* crystallization of celsian, α to β phase transformation, microstructures and properties, were examined. The use of a pre-synthesized celsian as a raw material was found to enhance the rates of densification and phase transformation due to the excess silica from raw Si_3N_4 powders which, however, did not change the microstructure and crystallization behaviour of celsian. Increases in hot-pressing temperatures and times increased the total number of large elongated β grains and resulted in coincidental increases in strength and toughness until the α to β transformation was complete. An intermediate quench-and-reheat step during hot pressing made the microstructure finer and more uniform by greatly reducing the large-sized elongated β grains. The quenching step also disrupted complete crystallization of celsian which led to more grain-boundary glassy phase and compromised the material's high-temperature properties.

1. Introduction

Preparation of dense Si_3N_4 usually requires the use of additives which react with the surface oxide (SiO_2) present on Si_3N_4 to form a liquid phase that facilitates densification. Various compounds can be used as additives. Negita [1, 2] selected oxide additives based on thermodynamic considerations. Many of them have been successfully demonstrated to produce dense Si_3N_4 materials [3–6]. In most cases, the additives in Si_3N_4 end up as a grain-boundary glass phase which softens and degrades the properties at high temperatures [7]. However, if properly engineered, the glass can be crystallized to improve the high-temperature properties [8].

A good additive system should form the liquid phase at a low temperature, i.e. a low liquid eutectic temperature, and the liquid phase later will be crystallized completely into a compound that has a high melting point. One such system which fulfils these requirements is the BaO–Al_2O_3–SiO_2 system. The three-component oxide system has a lowest liquid eutectic around 1175 °C [9] and forms a highly refractory compound, celsian ($BaAl_{2s}Si_2O_8$), which has a melting point of 1760 °C. Pickup and Brook [10, 11] used this concept and prepared a dense Si_3N_4 with 10 mol% celsian. They found crystalline celsian, instead of glass, formed *in situ* in a hot-pressed material which retained 60% of its three-point bend strength at 1400 °C and had good oxidation resistance. However, the material had a large amount of residual α-Si_3N_4 which limited its room-temperature strength to 530 MPa.

This work was undertaken to improve the mechanical properties of Si_3N_4/celsian ceramics by varying the celsian sources and the hot-pressing conditions. The effects of these parameters on densification, *in situ* crystallization of celsian, α to β phase transformation, microstructure and mechanical properties, were examined.

2. Experimental procedure

2.1. Material preparation

Two different Si_3N_4/celsian compositions (M1 and M2) were fabricated and tested. Each was formulated based on an addition of 10 wt % celsian (Table I). The additives in composition M1 consisted of BaO, Al_2O_3 and SiO_2. The first two oxides and the sum of added and surface SiO_2 from Si_3N_4 powders were calculated to form a stoichiometric celsian. Composition M1 was similar to that prepared by Pickup and Brook [11] but differed in two areas from the formulation in Pickup and Brook's work: (1) no excess BaO and Al_2O_3 were used, and (2) instead of $Ba(NO_3)_2$, BaO was used. Composition M2 was prepared by using an in-house presynthesized celsian powder as the sole additive. The celsian powder was fabricated by calcining a co-precipitated Ba–Al–Si hydroxide mixture. Because the surface SiO_2 from Si_3N_4 could

* Author to whom all correspondence should be addressed.
§ *Present address*: Highlight Optoelectronics, Inc., S.B.I.P., Hsin-Chu, Taiwan, R.O.C.

0022–2461 © *1996 Chapman & Hall*

TABLE I Material compositions (wt%)

Composition	Si_3N_4	BaO	Al_2O_3	SiO_2	Celsian
M1	91.85	4.17	2.77	1.21	–
M2	90.00	–	–	–	10.00

Si_3N_4, UBE SN-E10; BaO, Alpha Product; Al_2O_3, Reynold RC-HPDBM; SiO_2, Cabot fumed silica.

not be compensated for in this case, the overall oxide composition did not form a stoichiometric celsian and the total glass content was slightly higher in composition M2 than in M1.

The designated powder mixtures were attrition milled for 1 h in methanol using ZrO_2 ball media. The milled slurry was dried and sieved through a 60-mesh screen. The dry powder was hot pressed at 1750–1925 °C for various times in a BN-coated graphite die under flowing nitrogen. The hot-pressing pressure was 35 MPa. The heating rate varied between 25 and 45 °C min^{-1}. Rapid cooling was accomplished by circulating chilled water through the furnace and increasing the nitrogen purging. The cooling rate was greater than 100 °C min^{-1} for the first 3 min. The temperature dropped to around 1350 °C in the first 5 min cooling period. A computer was used to record all the hot-pressing variables, including ram displacement, temperature, pressure and time. From these data, the densification behaviour of the different materials was characterized and compared.

2.2. Material characterization

Densities of the hot-pressed billets were measured by the water immersion method. A slice of the billet was polished for phase analysis and Vicker's hardness. X-ray diffractometry ($CoK\alpha_1$) was used for phase analysis. Quantitative phase analyses of Si_3N_4 and celsian were obtained by comparing the peak intensity ratios as described previously [11, 12]. Possible solid-solution formation in β-Si_3N_4 and celsian was verified by changes in the lattice parameters. For lattice parameter refinement, either silicon or LaB_6 was used as an internal line position standard. Hardness was measured by a Vicker's diamond indentor using a load of 14.5 kg from a surface parallel to the hot-pressing direction. Flexural strength and fracture toughness data were collected using 3 mm × 4 mm × 45 mm bend bars. Four-point bend strength was determined at ambient and elevated temperatures in air. Chevron-notch toughness was measured with a three-point fixture and a loading rate of 1 μm min^{-1}. In both cases, the crack propagation direction was parallel to the hot-pressing direction. General microstructures were examined from the fracture and polished surfaces by scanning electron microscopy (SEM). Detailed characterization of the secondary and grain-boundary phases was investigated by transmission electron microscopy (TEM) and energy dispersive spectroscopy (EDS).

3. Results

3.1. Densification behaviour

By varying the hot-pressing conditions, four different materials were generated from compositions M1 and M2. Table II lists their densities, hot-pressing characteristics (i.e. densification temperature and time) and the corresponding hot-pressing conditions. All four materials densified readily and achieved full density. Fig. 1 shows a typical densification curve.

However, differences in densification behaviour existed among the four materials. The differences were manifested when two indicators, derived from the hot-pressing data, were compared. One is the onset temperature, T_s, where rapid densification took place during hot pressing. The other is the time, Δt, required for complete densification at the soak temperature. The measured T_s and Δt are listed in Table II. The implications of these two indicators on the densification behaviour have been discussed previously [13]. A combination of low T_s and small Δt usually signifies a system that densifies quite readily. Taking the material M1A as a reference, the following observations were made. Using presynthesized celsian powders as an additive (i.e. material M2A) markedly raised the densification on-set temperature, T_s. The T_s was delayed by more than 100 °C. However, the time required to full densification, Δt, was reduced to one-third the time required to densify material M1A. A likely scenario to explain this phenomenon is that the celsian melted late, because of its high melting point (1760 °C), which delayed the liquid formation and thus impeded the onset of densification. However, once it melted, a large amount of liquid phase formed instantaneously, which led to accelerated densification over a short period of time.

TABLE II Summary of hot-pressing results (see text for details)

Material	Composition	Hot-pressing[a]		T_s (°C)	Δt (min)	Density (g cm^{-3})
		(°C)	(h)			
M1A	M1	1825	1	1702	18	3.20
M1B	M1	1925	1	n.a.	n.a.	3.21
M1C	M1	1825	3[b]	n.a.	n.a.	3.21
M2A	M2	1825	1	1810	5.5	3.20

[a] Heating rate: 25 °C min^{-1} for M1A and M2A, 40 °C min^{-1} for M1B.
[b] A intermediate quench-and-reheat step was employed before the 1825 °C, 3 h soaking, where the material was first heated to 1925 °C at a rate of 45 °C min^{-1} and soaked for 15 min, followed by rapid cooling to 1450 °C and reheating back to 1825 °C at a rate of 21 °C min^{-1}.

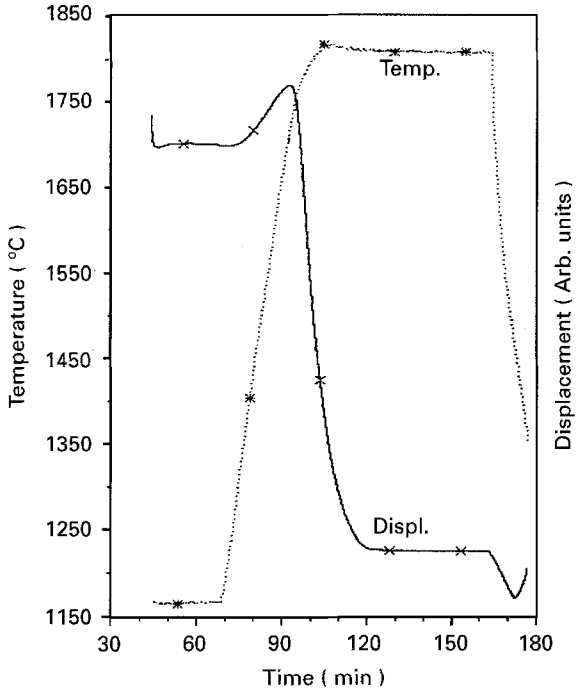

Figure 1 A typical hot-pressing curve of Si_3N_4/celsian materials.

3.2. Phase characterizations

Qualitative phase analyses showed only three crystalline phases in all of the materials, i.e. β-Si_3N_4, α-Si_3N_4 and hexacelsian. A typical XRD spectrum is shown in Fig. 2. Note that hexacelsian was formed *in situ* in the as-hot-pressed specimen without any heat treatment. *In situ* crystallization of hexacelsian must have occurred during the cooling stage of hot pressing. Similar phenomena have been observed previously [11]. Quantitative phase analyses, however, revealed differences in the four materials. Differences arose in two areas: (1) the extent of α and β Si_3N_4 phase transformation, and (2) the amount of hexacelsian. Table III is a summary of the amounts of residual α-Si_3N_4 and hexacelsian calculated from the integrated peak intensities from the XRD spectra. The amount of residual α-Si_3N_4 was calculated as follows [12]

$$\alpha(\text{wt }\%) = [I_{\alpha(102)} + I_{\alpha(210)}] / [I_{\alpha(102)} + I_{\alpha(210)} + I_{\beta(101)} + I_{\beta(210)}] \quad (1)$$

and the amount of hexacelsian was calculated with respect to Si_3N_4 content

$$\text{hexacelsian (wt }\%) = I_{hc} / (I_{\alpha-Si_3N_4} + I_{\beta-Si_3N_4} + I_{hc}) \quad (2)$$

TABLE III Contents of α-Si_3N_4 and hexacelsian calculated from XRD

	M1A	M1B	M1C	M2A
Residual α-Si_3N_4 (wt %)	42	3	5	25
Hexacelsian (wt %)	22	19	17	23

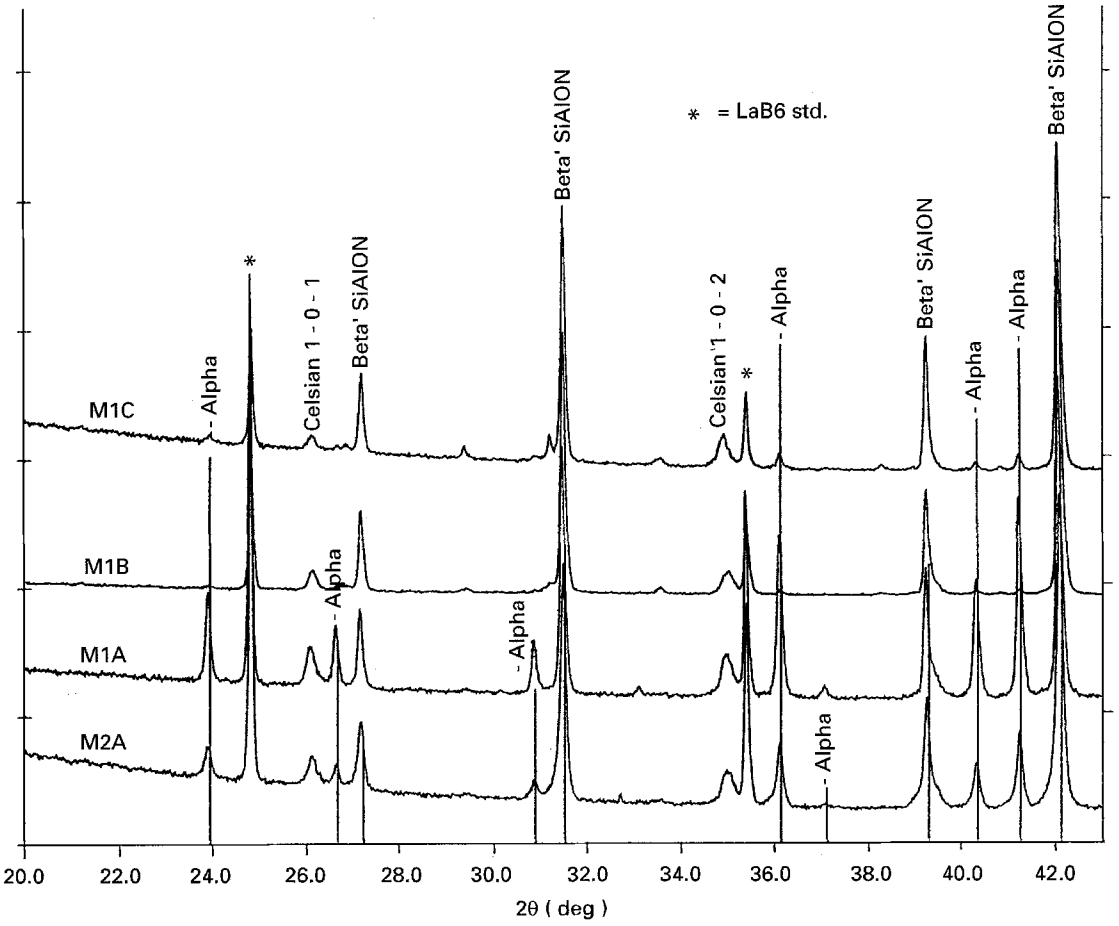

Figure 2 X-ray diffraction patterns of the four Si_3N_4-celsian materials.

TABLE IV Lattice parameters of the β phase

	M1A	M1B	M1C	M2A	β-Si_3N_4
a (nm)	0.76063	0.76065	0.76060	0.76057	0.76044
c (nm)	0.29105	0.29101	0.29098	0.29091	0.29075

where

$$I_{\alpha-Si_3N_4} = [I_{\alpha(102)} + I_{\alpha(210)}]/2 \quad (3)$$

$$I_{\beta-Si_3N_4} = [I_{\beta(101)} + [I_{\beta(210)}]/2 \quad (4)$$

and I_{hc} is the average intensity of (1 0 1) and (1 0 2) peaks of hexacelsian. There was 42% residual α-Si_3N_4 in the material M1A, whereas there was only 25% in the material M2A under the same hot-pressing conditions. A higher hot-pressing temperature or longer hot-pressing time reduced the residual α-Si_3N_4 significantly in materials M1B and M1C to $\leq 5\%$. On the other hand, the amount of hexacelsian was comparable in materials M1A and M2A, slightly lower in M1B, and noticeably lower in M1C. Higher temperatures and longer hot-pressing times appeared to hinder *in situ* crystallization of hexacelsian.

Lattice parameter data (Table IV) indicate that the β-Si_3N_4, referred to earlier in Fig. 2, was, in fact, a β-SiAlON, i.e. $Si_{6-x}Al_xO_xN_{8-x}$ ($x = 0$–4.27) [14], although the amount of aluminium substitution in the β-SiAlON was small, ranging from $x = 0.061$–0.099 (or 0.76–1.24 eq %), and varied in the four materials. Formation of β-SiAlON was also observed by Pickup and Brook [11], who reported an aluminium substitution at $x = 0.35$ (or 4.44 eq %). The much higher aluminium substitution found in their work could be a direct outcome of excess Al_2O_3 used in their material preparation.

3.3. Microstructures

Under the same hot-pressing conditions, the microstructures did not vary significantly with the use of presynthesized celsian. However, microstructures varied greatly with different hot-pressing conditions for the same composition. This is clearly illustrated by the microstructures in Fig. 3, where scanning electron micrographs were taken from fracture surfaces. For materials which contain a large amount of *in situ* crystallized hexacelsian, e.g. material M1A (hot-pressed at 1825 °C for 1 h), a typical microstructure is shown in Fig. 3a. The most dominant feature is the elongated β-SiAlON grains, followed by submicrometre-sized residual equiaxed α-Si_3N_4 grains, and lastly nanosized (average grain size on the nanometre level) irregular-shaped "speckles" of hexacelsian. The elongated SiAlON grains were bimodal in size (i.e. diameter). A larger portion had a diameter less than 0.3 μm and a smaller portion had a diameter at least twice that of the finer-sized population. Grains with a diameter greater than 1 μm were common. As the average size of grains grew, the population of large elongated grains increased. However, their diameter did not increase substantially. In contrast, the small elongated grains increased in diameter and not much in population. This is readily manifested by the microstructure of material M1B (hot pressed at 1925 °C for 1 h) in Fig. 3b. Depending on the quantity of residual α-Si_3N_4, the population of equiaxed grains varied. For example, there were more in material M2A than in M1A. The nanosized hexacelsian, confirmed by analytical TEM, was distributed rather uniformly throughout the material. The combined features of nanosize, distribution uniformity and *in situ* formation of the hexacelsian make the Si_3N_4/celsian material rather unique. In fact, it satisfies several attributes mentioned for a new-generation of materials [15].

Microstructures were also changed by varying the hot-pressing conditions. This was particularly apparent when hot-pressing was interrupted by a sudden drop of temperature (or quench), followed by an immediate temperature recovery. For example, in the material M1C (see Table II), the quench-and-reheat resulted in a finer and more uniform microstructure (Fig. 3c). As in the M1A material, most grains in this material were elongated. However, the grain diameter was typically < 0.3 μm and grains with diameter > 1 μm were rarely seen. Furthermore, the nanosized hexacelsian particles were not readily found. This correlated with the marked decrease in the content of hexacelsian in this material (see Table III).

3.4. Properties

3.4.1. Hardness and fracture toughness

Vicker's hardness varied with differences in phase composition and microstructure, although the variation was within 10%, ranging from 1571–1730 kg mm^{-2} (Table V). Hardness appeared to increase with increasing residual α-Si_3N_4 content and decreasing grain size. Similar observations have been cited in the literature [13]. The relationships were most obvious for materials of identical composition which were processed under different hot-pressing conditions, as in the M1 series. Material M1A had the highest hardness due to its high α-Si_3N_4 content (42%) and fine grain size. Despite a similar α-Si_3N_4 content ($\leq 5\%$), material M1C was harder than material M1B because of its smaller grain size. Material M2A, which was prepared using presynthesized celsian, had a low hardness despite its high α-Si_3N_4 content (25%) and fine grain size. The lower hardness could be due to the excess SiO_2 in this material.

In contrast, fracture toughness was mainly affected by differences in microstructure, specifically the quantity and size of elongated grains. The fracture toughness data in Table V illustrate this point. Material M1B, which had the greatest number of large-sized elongated grains gave the highest toughness (Fig. 3b). The exact opposite was true for material M1A, which had the fewest elongated grains and finest grain size (Fig. 3a). Material M1C had a lower toughness than material M1B, again due to its fine grain size (Fig. 3c).

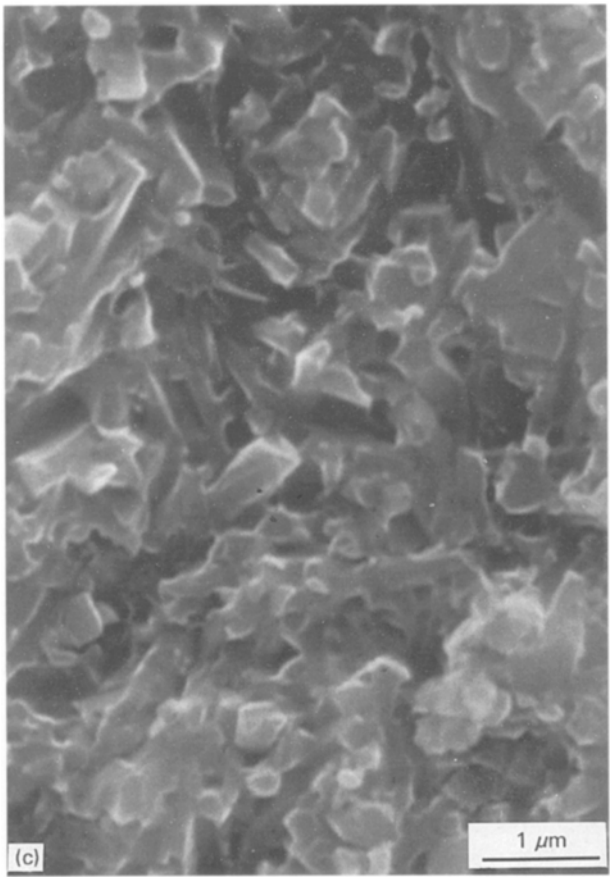

Figure 3 Microstructures of Si_3N_4-celsian materials: (a) M1A material, (b) material M1B and (c) material M1C.

TABLE V Summary of mechanical properties of the four materials

Material	Vicker's hardness ($kg\,mm^{-2}$)	Fracture toughness ($MPa\,m^{1/2}$)	Flexural strength	
			25 °C (MPa)	1375 °C (MPa)
M1A	1730 ± 39	4.5 ± 0.2	703 ± 105	431 ± 65
M1B	1571 ± 0	6.9 ± 0.1	817 ± 181	498 ± 17
M1C	1634 ± 0	5.9 ± 0.1	733 ± 61	356 ± 91
M2A	1596 ± 26	5.3 ± 0.2	804 ± 93	412 ± 10

3.4.2. Flexural strength

The room-temperature flexural strength of the materials followed a trend similar to that observed for fracture toughness (Table V). Strength increased with increasing numbers of elongated β grains. This is illustrated by comparing materials M1A and M1B. It should be noted that the strength increase was accompanied by a concurrent increase in fracture toughness. This trend seemed to continue until all the α-Si_3N_4 was transformed to β phase. However, strength decreased slightly in material M1C where the average grain-aspect ratio was reduced by the intermediate quench-and-reheat step. This was true regardless of its finer grain size. In any event, all of the strength data obtained here were higher than the value reported in Pickup and Brook's work (530 ± 20 MPa by a three-point bend method) where the material contained a higher residual α-Si_3N_4 content.

The strength at 1375 °C highlights the significance of complete *in situ* crystallization of hexacelsian. For materials with fully crystallized hexacelsian, strength was always greater than 400 MPa at 1375 °C.

Differences in the room-temperature strength had little effect on this. This suggests that the strength of these materials at 1375 °C depends more on the nature of the hexacelsian phase and less on that of Si_3N_4. This is further illustrated in materials that do not have the hexacelsian phase completely crystallized. Crystallization of hexacelsian in the material M1C was partially interrupted by the intermediate quench-and-reheat step. Incomplete crystallization of hexacelsian led to an excess amount of grain-boundary glass that compromised the high-temperature strength.

4. Discussion

4.1. *In situ* crystallization of hexacelsian

The liquid phase in the Si_3N_4/celsian system underwent an *in situ* crystallization upon cooling. The crystallization product was hexagonal celsian (or hexacelsian) and no monoclinic celsian was found. This phenomenon had been observed before by Pickup and Brook [11]. The *in situ* crystallization phenomenon was relatively hardy. It occurred with variable celsian contents, e.g. from about 20 wt % [11] to 10 wt % in this work. It could be obtained by using different starting raw materials, such as a mixture of $Ba(NO_3)$ (or BaO)-Al_2O_3–SiO_2 [11], presynthesized celsian (material M2A), and other systems which formed a solid solution of celsian [16]. The *in situ* crystallization was not affected by the presence of excess SiO_2 as in the case of material M2A.

Crystallization of hexacelsian was initiated by a homogeneous nucleation and followed by a slow growth due to exhaustion of the liquid phase. This resulted in formation of uniformly distributed nanosized hexacelsian particles along the Si_3N_4–Si_3N_4 grain boundaries throughout the material. This kind of microstructure has not often been observed for Si_3N_4-based materials when the grain-boundary liquid phase was crystallized. In most cases, the crystallized product existed either as pockets of large single-crystals extending over several Si_3N_4 grains [17, 18] or as isolated islands at the multi-grain junctions [19]. This unusual feature of *in situ* crystallization of uniformly distributed nanosized hexacelsian contributes to both the good room- and elevated-temperature properties of this material.

4.2. Effect of using presynthesized celsian

Use of presynthesized celsian ($BaAl_2Si_2O_8$) as an additive (i.e. the M2 system) differs in one aspect from that of using additives of BaO, Al_2O_3 and SiO_2 which were formulated as a stoichiometric celsian (i.e. the M1 system). The surface SiO_2 from the raw Si_3N_4 could be compensated for by reducing the starting SiO_2 in the M1 system but not in the M2 system. Therefore, there is more liquid formed in the M2 system when a constant amount of celsian is used. In addition, the liquid in the M2 system would be less viscous than in the M1 system owing to a higher oxygen content [20]. These two factors explain why the material M2A took less time to densify (i.e., shorter Δt) and had more α-Si_3N_4 transformed to β-Si_3N_4 than the M1A material. However, the rapid densification onset temperature, T_s, was higher for the material M2A than for M1A. This is owing to a higher liquid eutectic temperature for the material M2A. The lowest eutectic temperature for the material M1A is 1175 °C, as determined by the three-component system of BaO–Al_2O_3–SiO_2 [9]. The eutectic temperature for the material M2A is 1311 °C, as determined by the two-component system for $BaAl_2Si_2O_8$–SiO_2 [21].

The excess SiO_2 in the M2 system had a minimal effect on microstructural development and properties. Under the same processing conditions, the microstructures of the M1A and M2A materials were difficult to distinguish. With the exception of hardness, their properties were comparable. The slightly higher strength and toughness of material M2A is due to its increased number of elongated β-Si_3N_4 grains. The *in situ* crystallization of hexacelsian was not affected by the excess SiO_2 in material M2A. The XRD results showed nearly the same amount of hexacelsian in materials M1A and M2A. The excess SiO_2 in the material M2A led to more non-crystallized amorphous grain-boundary phase. This could account for its lower hardness and slightly increased fracture toughness.

4.3. Effects of hot-pressing conditions

Hot-pressing conditions greatly affect the microstructure and thus material properties. Conditions which allow full development of interlocking elongated microstructures in Si_3N_4 materials yield better properties [22]. These conditions vary for different material compositions. For the Si_3N_4/celsian system, the kinetics of α to β phase transformation are sluggish compared to most of other Si_3N_4 systems [13, 18, 23, 24]. Higher temperatures and/or longer hot-pressing times are required to obtain full transformation. This is readily shown in Fig. 4, where room-temperature flexural strength and β content are plotted against the hot-pressing temperature. Although the material could be densified fully after 1 h at $\leq$ 1750 °C, the best overall properties were achieved at 1925 °C, where residual α-Si_3N_4 was $\leq$ 5%.

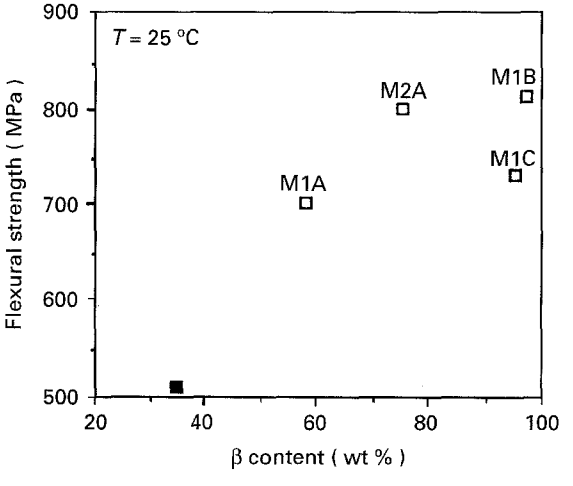

Figure 4 Flexure strength as a function of α to β phase transformation. (■) Pickup and Brook [10, 11].

The aforementioned phenomenon can be easily altered by an interruption in the heating stage of hot pressing. The current work showed that a quench imposed during the early stages of phase transformation altered the subsequent microstructural evolution and glass crystallization. The Si_3N_4 microstructure became finer and more uniform in size distribution. Complete *in situ* glass crystallization was either retarded or curtailed. This result had an adverse effect on the material properties.

Finally, it is interesting that with minimal effort, the Si_3N_4/celsian material has exhibited properties comparable to those for some of the best-known high-temperature Si_3N_4 materials to date [13, 19, 25–27]. The good properties, coupled with the unique *in situ* glass crystallization characteristics (that translate to a simpler material preparation), demand this material be seriously considered for applications at elevated temperatures.

5. Conclusions

Four types of Si_3N_4 ceramic with celsian as an additive have been prepared by hot pressing using different celsian raw-material sources and hot-pressing conditions. The following observations were noted.

1. Regardless of celsian sources and hot-pressing conditions, the liquid phase formed at elevated temperatures crystallized *in situ* into hexacelsian during cooling after hot pressing. The hexacelsian phase was uniformly distributed as nanosized particles at the Si_3N_4–Si_3N_4 grain boundaries. Excess SiO_2 from raw Si_3N_4 did not affect the crystallization of hexacelsian, whereas an intermediate quench-and-reheat step during hot processing reduced the amount of crystallized hexacelsian.

2. Typical microstructures of Si_3N_4/celsian ceramics, which were not affected by the use of presynthesized celsian, consisted of nanosized hexacelsian particles, fine equiaxed residual α-Si_3N_4 grains, and large (> 0.50 μm diameter) and small (< 0.3 μm diameter) elongated β-SiAlON grains which contained 0.76–1.24 eq % Al. The large elongated grains, which increased in population with increasing hot-pressing temperatures and residence times, were markedly reduced by an intermediate quench-and-reheat step.

3. The use of presynthesized celsian as a raw material had less effect on properties than the hot-pressing conditions. Vicker's hardness (from 1570–1730 $kg\,mm^{-2}$) of Si_3N_4/celsian materials was affected by the amount of residual α-Si_3N_4 and grain size. Fracture toughness (from 4.5–6.9 MPa $m^{\frac{1}{2}}$) and room-temperature flexure strength (from 703–817 MPa), usually opposite in trend to hardness, were affected mainly by the size and quantity of elongated grains. Both toughness and strength increased with increasing grain size until completion of the α to β phase transformation. High-temperature flexural strength 356–498 MPa at 1375 °C), however, was predominantly determined by the amount of *in situ* crystallized hexacelsian. Strength was degraded by an intermediate quench-and-reheat step during the hot-pressing procedure which reduced the amount of crystallized hexacelsian.

Acknowledgements

The authors thank J. R. Moyer for supplying the presynthesized celsian powder, H. E. Rossow, S. M. Fuller and M. B. Rice for experimental assistance, and D. R. Howard and A. M. Hart for reviewing the manuscript.

References

1. K. NEGITA, *J. Mater. Sci.* **4** (1985) 417.
2. *Idem, ibid.* **4** (1985) 755.
3. G. G. DEELEY, J. M. HERBERT and N. C. MOORE, *Powder Metall.* **8** (1961) 145.
4. G. E. GAZZA, *J. Am. Ceram. Soc.* **56** (1973) 62.
5. I. C. HUSBY and G. PETZOW, *Power Metall. Int.* **6** (1974) 17.
6. K. S. MAZDIYASNI and C. M. COOKE, *J. Am. Ceram. Soc.* **57** (1974) 536.
7. R. NATHAN and G. E. GAZZA, in "Nitrogen Ceramics," edited by F. L. Riley (Noordhoff, Leyden, 1977) p. 417.
8. K. KOMEYA, M. KOMATSU, T. KAMEDA, Y. GOTO and A. TSUGE, *J. Mater. Sci.* **26** (1991) 5513.
9. R. H. THOMAS, *J. Am. Ceram. Soc.* **33** (1950) 35.
10. H. PICKUP and R. J. BROOK, in "Ceramic Materials and Components for Engines", edited by W. Bunk and H. Hausner (Elsevier, London, 1986) p. 93.
11. H. PICKUP and R. J. BROOK, *Proc. Br. Ceram. Soc.* **38** (1988) 69.
12. D. R. MESSIER, F. L. RILEY and R. J. BROOK, *J. Mater. Sci.* **13** (1978) 1199.
13. C. J. HWANG, K. YANG, D. R. BEAMAN and H. E. KLASSEN, *Ceram. Eng. Sci. Proc.* **13** (1992) 1032.
14. L. J. GAUCKLER, S. PRIETZEL, G. BODEMER and G. PETZOW, in "Nitrogen Ceramic", edited by F. L. Riley (Noordhoff, Leyden, 1977) p. 529.
15. D. P. THOMPSON, *Mater. Res. Soc. Symp. Proc.* **287** (1993) 79.
16. C. J. HWANG and R. A. NEWMAN, *J. Eur. Ceram. Soc.*, in review.
17. D. A. BONNEL, M. RÜHLE and T. Y. TIEN, *J. Am. Ceram. Soc.* **69** (1986) 623.
18. C. J. HWANG, D. R. BEAMAN, R. A. NEWMAN, D. W. SUSNITZKY and A. J. PYZIK, *ibid.*, to be published.
19. A. P. TAGLIALAVORE, E. BRIGHT, B. J. MCENTIRE, W. T. COLLINS, S. A. DYNAN, L. D. LYNCH and R. F. GIRVIN, in "Proceedings of The Annual Automotive Technology Development Contractors' Coordination Meeting", (SAE, Warrendale, PA, 1993) p. 277.
20. W. D. KINGERY, H. K. BOWEN and D. R. UHLMANN, "Introduction To Ceramics" (Wiley, New York, 1976).
21. H. C. LIN and W. R. FORSTER, *Am. Mineral.* **55** (1968) 134.
22. Z. ZIEGLER, J. HEINRICH, and G. WOTTING, *J. Mater. Sci.* **23** (1988) 3412.
23. D. R. MESSIER and F. L. RILEY, in "Nitrogen Ceramics," edited by F. L. Riley (Noordhoff, Leyden, 1977) p. 141.
24. C. M. HWANG and T. Y. TIEN, in "Sintering '87," edited by S. Somiya, M. Shimada, M. Yoshimura and R. Watanabe (Elsevier, UK, 1988) p. 1034.
25. C. J. HWANG, S. M. FULLER and D. R. BEAMAN, *Ceram. Eng. Sci. Proc.* **15** (1994) 685–93.
26. H. YEH, J. YAMANIS, C.-W. LI, J. POLLINGER, E. SOLIDUM and M. BEHI, in "Proceedings of The Annual Automotive Technology Development Contractors' Coordination Meeting", (SAE, Warrendale, PA, 1993) p. 465.
27. G. V. SRINIVASAN, S. K. LAU and R. S. STORM, *ibid.*, p. 451.

Received 26 July 1994
and accepted 7 June 1995